Article:
Fuller, AJ, Shaw, S, Peacock, CL et al. (2 more authors) (2016) EXAFS Study of Sr sorption to Illite, Goethite, Chlorite, and Mixed Sediment under Hyperalkaline Conditions. Langmuir, 32 (12). pp. 2937-2946. ISSN 0743-7463

https://doi.org/10.1021/acs.langmuir.5b04633

EXAFS Study of Sr sorption to Illite, Goethite, Chlorite, and Mixed Sediment under Hyperalkaline Conditions

Adam J. Fuller[†], Samuel Shaw[‡], Caroline L. Peacock[†], Divyesh Trivedi[§], and Ian T. Burke[*†]
[†] School of Earth and Environment, University of Leeds, Leeds LS2 9JT, United Kingdom
[‡] School of Earth, Atmospheric and Environmental Science, University of Manchester, Manchester M13 9PL, United Kingdom
[§] National Nuclear Laboratory Ltd, Chadwick House, Warrington Road, Birchwood Park, Warrington WA3 6AE, United Kingdom
Langmuir, Article ASAP
DOI: 10.1021/acs.langmuir.5b04633
Publication Date (Web): March 03, 2016

*Tel: +44113 3437532. E-mail: i.t.burke@leeds.ac.uk.

Abstract

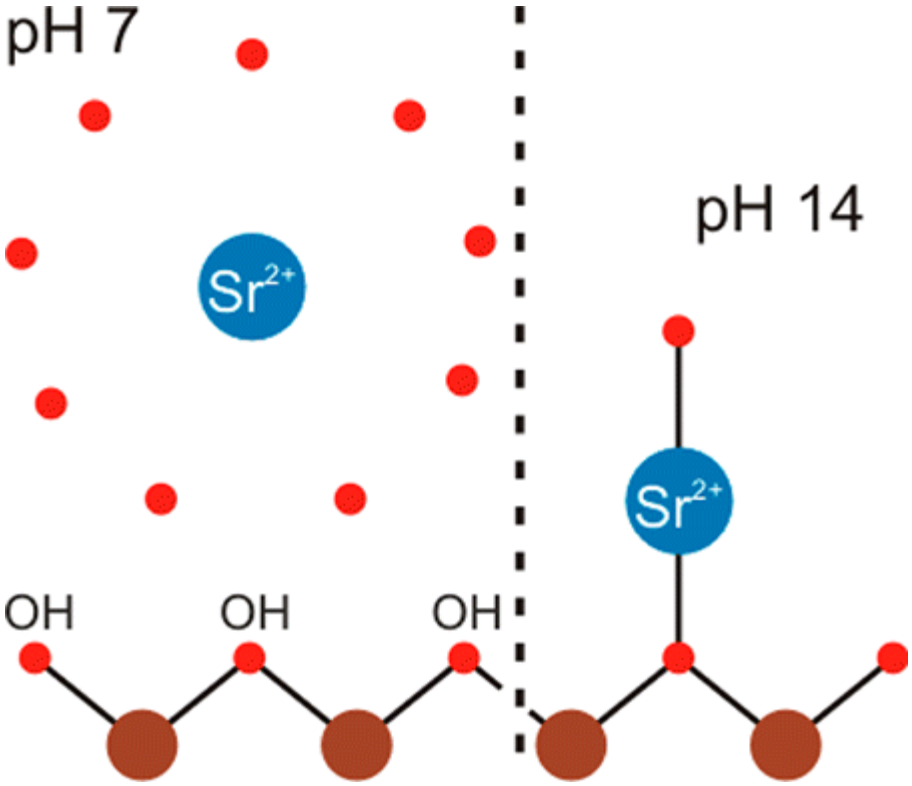

Strontium is an important contaminant radionuclide at many former nuclear sites. This paper investigates the effect of changing pH and ionic strength on the sorption of Sr to a range of common soil minerals. Specifically it focuses on the sorption of Sr onto illite, chlorite, goethite, and a mixed sediment. The interplay between ionic strength and pH was determined

by varying the background ionic strength of the system using both NaCl (for a constant pH) and NaOH (to also vary pH). Under conditions of moderate pH, Sr sorption decreased with increasing ionic strength, due to competition between the Na and Sr atoms for the outer-sphere complexes. However, where increasing ionic strength was accompanied by increasing pH, Sr sorption remained high. This suggested that Sr was sorbed to the minerals without competition from background Na ions. Extended X-ray absorption fine structure (EXAFS) spectra confirmed that at highly alkaline pH (>12.5) Sr was forming inner-sphere complexes on the surfaces of all minerals. This specific adsorption of the Sr (as $SrOH^{+}$) explains why it was still adsorbed to the minerals under very high ionic strength conditions and was not out-competed by Na.

-

1 Introduction

The widespread use of nuclear power over roughly the last 50 years has left a large volume of radioactive nuclear waste. This waste is present in many forms, both solid and liquid, and contains a wide range of both actinides (e.g., ^{238}U, ^{240}Pu) and fission products (e.g., ^{90}Sr, ^{137}Cs, ^{99}Tc). This study focuses specifically on ^{90}Sr which is produced in high yield by nuclear fission and is present in large concentrations in nuclear waste. With a half-life of 29 years, ^{90}Sr is classified as a medium-lived radionuclide and decays via β-emission to ^{90}Y, which is also a high energy beta emitter. Historic leaks and authorized discharge from nuclear facilities have released ^{90}Sr (and other radionuclides) into the geosphere. This poses a potential risk to the environment and to human health. Therefore, it is essential to understand and be able to predict the behavior of Sr in the terrestrial environment.
Under normal environmental conditions ^{90}Sr is present as the aqueous Sr^{2+} cation. The mobility of Sr^{2+} in the environment is chiefly controlled by sorption to the charged surfaces of minerals. Sorption of Sr^{2+} to common mineral phases in soils under moderate environmental conditions (low ionic strength, pH 4–10) is well understood. Under these conditions, Sr primarily sorbs to those minerals with large surface area and cation exchange capacity, chiefly clays and iron oxides.(1-4) Sorption is known to occur at circumneutral pH though charge compensating cation exchange with the Sr^{2+} cation exchanging with other mono- and divalent cations in outer-sphere surface complexes.(3, 5-9) This outer-sphere sorption occurs in competition with other mono and divalent cations and is therefore strongly controlled by the ionic strength (IS) of the solution phase.(10, 11) Strontium sorption is significantly reduced in high ionic strength solutions as the other ions present (such as Na^{+}) out-compete Sr^{2+} for the sorption sites.(12)
Due to use of alkaline liquors in waste treatments (such as at Hanford and Sellafield) significant quantities of the Sr bearing wastes have a hyper-alkaline pH and a high ionic strength.(13, 14) Additionally, the use of cementitious materials is widely proposed in geological disposal facilities (both for waste encapsulation and as a backfill).(15) The long-term interaction of groundwater with cement is known to lead to the development of high pH, high ionic strength plumes, rich in Ca. It is therefore also important to understand the sorption of Sr, and other alkali-earths, under these hyperalkaline conditions. It is well established that the long-term interaction of high pH solutions with silicate minerals leads to their dissolution and reprecipitation as neoformed zeolite phases and calcium-silicate-hydrates.(16-20) Strontium readily incorporates into these phases, leading to its long-term immobilization.(21, 22) These transformation and incorporation reactions take long time periods under surface pressure and temperature conditions.(23) However, Wallace et al.(24)

observed that Sr sorption is also enhanced in high pH solutions over the short term, before these new phases can form. They observed that Sr sorption at high pH was unaffected by cationic competition at high ionic strength and proposed that this was due to formation of an inner-sphere surface complex. The formation of a Sr–Fe inner-sphere complex on goethite at pH 10 was also previously observed by Collins et al.(25) In both of these cases, the authors were able to determine this transition from outer-sphere to inner-sphere surface complexation using EXAFS. This confirms the utility of this technique for identifying the nature of the Sr sorption complex at the molecular scale.

This paper builds on these discoveries to fully determine the sorption mechanism accounting for enhanced Sr sorption at high pH over the short-term. Here the sorption of Sr to illite, goethite and chlorite was investigated across a range of pH and ionic strength conditions. The experiments were run for 48 h to allow sorption equilibration but to minimize any mineral alteration. As zeolite formation is known to take many months,(23) this short time period ensured that the results from this study were limited to sorption processes rather than incorporation. The study aimed to determine whether Sr forms inner-sphere complexes on mineral surfaces, and at which pH this transition from outer-sphere to inner-sphere adsorption occurred. A mechanistic explanation for the complexation process and its implications for the behavior of other alkali-earths is then offered.

2 Materials and Methods

2.1 Materials Preparation

A sample of illite IMT-1 was obtained from the Clay Minerals Society Source Clay Repository. This is a well characterized source clay with the formula $(Mg_{0.09}\ Ca_{0.06}K_{1.37})$ $[Al_{2.69}Fe(III)_{0.76}Fe(II)_{0.06}Mntr\ Mg_{0.43}Ti_{0.06}]$ $[Si_{6.77}Al_{1.23}]O_{20}(OH)_4$. It is cation exchange capacity (CEC), was previously reported as 15 mequiv 100 g^{-1}.(26) A sample of chlorite (clinochlore) was purchased from Ward's Natural Science Establishment. This has the general formula $(Mg, Fe)_5Al(Si_3Al)O_{10}(OH)_8$ and a CEC of 3.8 mequiv 100 g^{-1}.(27) Goethite was synthesized in the lab following the method of Schwertmann and Cornell(28) and has the general formula FeO(OH). The purity of the minerals was confirmed by XRD (Figure S1). The sediment was collected in August 2009 from the Calder Valley, Cumbria. It is mineralogical composition was previously determined by Wallace et al.(29) and Law et al.(30) and is known to contain illite, chlorite, and iron oxides and has a CEC of 8.2 mequiv 100 g^{-1}.(29)

All materials were crushed to <63 μm (verified by sieving). To remove any carbonate present the samples were washed in 0.001 mol L^{-1} HCl for 2 h on a rotary shaking table in beakers open to the atmosphere (to allow evacuation of CO_2). Solid solution separation was achieved by centrifugation at 6000g for 5 min. The supernatant was then discarded and the solids rinsed three times with deionized water (repeating the centrifugation procedure each time). Finally, the samples were oven-dried at 40 °C until excess water had evaporated.

2.2 Batch Sorption Reactions

As Sr is known to readily precipitate as $SrCO_3$ at high pH, great care was taken to exclude carbonate from the system. Solutions of degassed (CO_2 and O_2 free) NaCl and NaOH at concentrations ranging from 10^{-5} to 1 mol L^{-1} were prepared in glass Schott bottles. For this, deionized water was degassed for 30 min L^{-1} by bubbling with N_2 while constantly stirring at 90 °C on a hot plate. Following the initial degassing period, the relevant mass of NaOH or NaCl was added to the deionized water while degassing continued. Additionally, 2.5×10^{-4}

mol L^{-1} Ca (as $CaCl_2 \cdot 2H_2O$) was added to all solutions to precipitate any carbonate which was not removed as CO_2 by the degassing procedure. The solutions were then degassed for another 30 min L^{-1} before being transferred to a coy cabinet anaerobic chamber (with CO_2 concentrations <40 ppm). Both a 0.05 mol L^{-1} and a 0.02 mol L^{-1} solution of Sr (as $SrCl_2 \cdot 6H_2O$) were also prepared by the same degassing procedure but Ca was not added. All sample handling was then performed inside the anaerobic chamber. The minerals were suspended in NaOH and NaCl at a solid solution ratio of 0.8 g 35 mL^{-1} in 40 mL Oak Ridge centrifuge tubes. Solutions were filtered through a 0.45 μm filter before addition to the solids. This was to ensure removal of any $CaCO_3$ which may have precipitated during the solution preparation. Although the assumption was made at this stage that the majority of the Ca was removed as $CaCO_3$ by filtration a small fraction may have remained present in the solutions leading to a slight elevation of the total ionic strength (IS) compared to the Na concentration. The samples were then spiked with a hundred fold dilution of the 0.02 mol L^{-1} Sr solution to yield 2×10^{-4} mol L^{-1} Sr in the following samples: illite, all NaCl samples; chlorite all NaCl samples, 10^{-3} and 10^{-5} mol L^{-1} NaOH; goethite, all NaCl samples and 10^{-5} mol L^{-1} NaOH; sediment 10^{-5} mol L^{-1} NaOH and 10^{-1} mol L^{-1} NaOH. All other samples contained a 100-fold dilution of the 0.05 mol L^{-1} Sr solution to yield 5×10^{-4} mol L^{-1} of Sr in solution. Samples were then sealed and equilibrated for 48 h on a rotary shaker. During equilibration samples remained in the CO_2 free atmosphere to prevent any carbonate formation. Following the equilibration period the samples were transferred unopened from the chamber to a −80 °C freezer and frozen to suspend the sorption reaction.

2.3EXAFS Spectra Collection

The frozen samples were transported to the synchrotron in a N_2 purged airtight Kilner jar to minimize any CO_2 ingress and with ice packs to prevent defrosting. During the beam time, all samples were stored in a freezer and defrosted as needed prior to sample preparation. Before mounting the samples the tubes were defrosted, centrifuged and the supernatant was decanted. Supernatant pH was determined using a glass bulb electrode calibrated to pH 7 and 10 and 12 with standard calibration solutions. The solutions were then refrozen to minimize CO_2 ingress prior to analysis. The wet paste was then mounted in a Perspex sample holder and sealed with Kapton tape windows. The sample was then immediately frozen by immersion in liquid nitrogen. To minimize exposure to atmospheric CO_2 during mounting the material was kept under a constant flow of N_2 until it was frozen.

The Sr EXAFS data presented here were gathered from three distinct beamline sessions. Spectral data for the chlorite samples with 10^{-5}, 10^{-2}, and 10^{-1} mol L^{-1} NaOH and the sediment exposed to 10^{-1} mol L^{-1} NaOH were gathered at beamline B18 at the Diamond Light Source. Here the incident beam has a typical operating voltage of 3 GeV and a current of 300 mA. The X-rays at B18 are generated from a bending magnet source. The beam is vertically collimated by a Si mirror before passing through a double crystal Si monochromator. It was then focused onto the sample to give a spot size of 200 × 250 μm. The Sr K edge (16105 keV) EXAFS spectra were gathered from fluorescence X-rays using a 9 element Ge solid state detector. The sample was held at 80 K in a liquid nitrogen cryostat during data collection to improve the signal-to-noise ratio. The EXAFS data for samples of chlorite, goethite, sediment and illite in a 1 mol L^{-1} NaOH background and the chlorite sample in 10^{-5} mol L^{-1} NaOH were gathered at the Dutch Belgian Beamline (DUBBLE) at the European Synchrotron Radiation Facility (ESRF). This has an incident beam voltage of 6.04 GeV and a current of 200 mA. DUBBLE uses a bending magnet source which is vertically collimated by a Si mirror. The correct beam energy is then selected using a double crystal Si monochromator. The final incident beam has a spot size of 400 × 350 μm. Again at the ESRF a 9 element Ge detector was used to gather Sr K-edge fluorescence spectra. Data collection was also performed at 80 K in a liquid nitrogen cooled cryostat. Finally Sr K-edge

EXAFS data from samples of illite in 10^{-3} and 10^{-1} mol L NaOH and Goethite in 10^{-5}, 10^{-3} and 10^{-1} mol L NaOH were gathered at beamline I20 at the Diamond light source. Here the X-ray source is derived from a wiggler insertion device. The energy of the collimated beam is then selected by a unique 4 crystal monochromator which yields beam with very high energy stability. The monochromated beam is then focused to give a final spot size of 400 × 350 μm. Sr K-edge fluorescence spectra were gathered using a 64 element solid state Ge detector and samples were held in a liquid nitrogen cryostat at 80 K.

2.4EXAFS Data Analysis and Fitting

Multiple XAS scans from each sample were summed and averaged using Athena v 0.8.056(31) to maximize the signal/noise ratio. The background subtraction of the Sr EXAFS was then performed using PySpline v1.1.(32) The EXAFS spectra were then fitted in k-space using DLexcurv v1.0(33) following full curved wave theory.(34) Ab initio calculations of the phaseshifts were performed using the Hedin–Lundqvist potentials and assuming the von Barth ground states for all atoms.(35) Shell-by-shell fitting was then performed by estimating initial parameters for shells of backscattering atoms and then interactively refining these parameters. Specifically, fits were determined by refining number of atoms (±25%), interatomic distances (±0.02 Å in the first shell and ±0.05 Å in subsequent shells), Fermi energy, and Debye–Waller factor ($2\sigma^2$, ± 25%). This procedure was performed initially with a single shell and subsequent shells of surrounding atoms were then added. Additional shells were then accepted where they improved the overall fit quality by greater than 5% (determined by reduction of the least squared residual, R-factor).

2.5ICP-OES

The concentration of Sr sorbed to the solid phase was determined as initial $[Sr]_{aq}$ – final $[Sr]_{aq}$. The final concentration of Sr in solution after the 48 h sorption period was determined by ICP-OES. The frozen solutions were defrosted in the anaerobic chamber and diluted into 10% HNO_3 to acidify them. Dilution was necessary due to the high ionic strength of the background Na electrolyte. The concentration of Sr in the diluted solutions was then measured and the final aqueous concentration in the sample calculated.

2.6Solution Speciation Modeling

Speciation of the alkali earth ions as a function of pH was modeled using PHREEQC.(36) In all cases, a simple model was used with 45 ppm of the relevant element (Ca, Sr, Ba, Ra) at a pH range of 9–14. No other solid or solution phases were included. The activity of the different species was then determined using the Debye–Hückel equation. For Ca, Sr, and Ba the modeling was performed using the PHREEQC thermodynamic database. However, no thermodynamic data for Ra is provided in this database so Ra modeling was performed using the HATCHES18 database.(37)

•

3 Results

3.1Solution

Figure 1 shows the total sorption of Sr onto the 4 minerals (a, illite; b, chlorite; c, goethite; d, sediment) after equilibration for 48 h. In all cases, the square data points show sorption of Sr from a background of NaCl and circles show sorption of Sr from a background of NaOH. Data is presented in terms of percentage sorption with increasing Na concentration. The average pH of the NaCl system (with all minerals, not sediment) was pH 9.1 ± 0.2. The pH varied greatly with changing NaOH concentration; in this case, the pH of each point is annotated on the figure. In all mineral systems increasing ionic strength of NaCl caused a

decrease in percent sorption of strontium onto the surface. However, the results for sorption in the NaOH system are very different. Here there was no trend toward decreasing Sr sorption with increasing ionic strength. In fact the opposite appears to be true with greater Sr sorption percentages at high NaOH ionic strengths than at lower. However, it should be noted that residual concentrations of Ca present in the low IS NaOH systems (10^{-5} and 10^{-4} mol L^{-1}) may have raised the total IS of the system and led to suppressed Sr sorption percentages. The minor decrease in Sr sorption in the 1 mol L^{-1} systems may reflect the saturation of the minerals reactive sites, as the total IS of the system is above the reported CEC (see Materials and Methods).

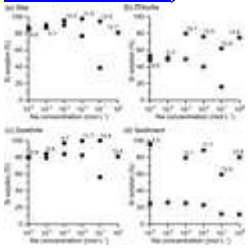

Figure 1. Sorption of Sr to (a) illite, (b) chlorite, (c) goethite, and (d) sediment as a function of Na concentration in a background of NaCl (squares) and NaOH (circles). The pH of the NaOH systems is annotated to clearly show the increase in pH with increasing concentration. All data points represent the average of a triplicate sample. Error bars are not shown where they were smaller than the symbol used.

In the illite system (Figure 1a) near total sorption of the Sr is seen in both the NaCl and NaOH system up to a total ionic strength of 10^{-3} mol L^{-1}. However, above this the effect of pH on Sr sorption is clear. In the NaCl system, the pH remained constant around 9.3 ± 0.07. Here the increasing ionic strength caused a large reduction in total Sr sorption from 90 ± 0.1% at 10^{-3} mol L^{-1} to 77 ± 0.4% at 10^{-2} mol L^{-1} and 39 ± 0.4% at 10^{-1} mol L^{-1} NaCl. Comparatively, in the NaOH system, the pH greatly increased with increasing NaOH concentration and the sorption of Sr remained high. Specifically, 94 ± 0.1% of the Sr sorbed to the mineral in 10^{-1} mol L^{-1} NaOH (pH 13). This is much more (40% greater sorption) than in the NaCl background at the same overall ionic strength. Even in the 1 mol L^{-1} NaOH system 80% of the Sr was sorbed to the illite.

The chlorite system showed more complex sorption behavior (Figure 1b). Here significantly more Sr was sorbed to the sediment in the NaOH system than in the NaCl system above an ionic strength of 10^{-4} mol L^{-1}. In the NaCl system the Sr sorption was reduced to 40 ± 1.1% at 10^{-2} mol L^{-1} and to 16 ± 0.8% at 10^{-1} mol L^{-1} NaCl. The pH in the NaCl system was constant at 9.1 ± 0.1. Comparatively in the NaOH system the pH increased greatly with increasing ionic strength, and Sr sorption remained high. At 10^{-3} mol L^{-1} NaOH (pH 10.7) 80 ± 0.3% of the Sr was sorbed to the sediment compared to 51 ± 0.3% at 10^{-5} mol L^{-1} NaOH (pH 9.3). This high Sr sorption was apparent even at 10^{-1} mol L^{-1} (pH 12.9) NaOH where 62 ± 0.9% of the Sr was sorbed. This is much greater than the Sr sorption from the same ionic strength solution at pH 9.2 (NaCl background). The sorption of Sr at 1 mol L^{-1} NaOH (pH 13.7) was even greater than at 10^{-1} mol L^{-1}, namely, 75%.

In the goethite system (Figure 1c), around 80% of the Sr was sorbed from the NaCl solutions up to and including 10^{-2} mol L^{-1}. The sorption of Sr decreased to 56 ± 2.4% in a 10^{-1} mol L^{-1} NaCl background. The average pH of the goethite NaCl system was 9.0 ± 0.32 across the concentration range. Comparatively the pH of the NaOH system greatly increased with increasing Na concentration. Here the percentage of Sr sorbed to the sediment remained constant at 98.8 ± 1.7% between 10^{-3} mol L^{-1} (pH 9.5) and 10^{-1} mol L^{-1} NaOH (pH 12.6).

This was much greater than in the comparative concentration of NaCl at pH 9. The total sorption of Sr decreased slightly at 1 mol L^{-1} NaOH (pH 13.6) to 81%.
The sediment system showed a significant pH buffering effect. Here it was found that all solutions with $<10^{-3}$ mol L^{-1} of NaOH buffered down to below pH 6.0. Wallace et al.(29) found that below pH 6.0 Sr sorption to the sediment was rapidly reduced. Therefore, any reported sorption data from below this pH sorption edge is likely to be affected by pH as well as ionic strength. The Sr sorption data to the sediment reported in Figure 1d was collected at pH 4.8 ± 0.3. Here the maximum Sr sorption percentage was 26% at 10^{-4} mol L^{-1} NaCl. This reduced concentration is likely due to the low pH rather than ionic strength. This was confirmed by comparison to results from experiments using pH 6.5 ± 0.5 buffered sediments (Figure S2(26)) where >90% Sr sorption occurred at Na concentrations up to $\sim 10^{-2}$ mol L^{-1}. However, the effect of ionic strength was still evident with total Sr sorption reducing to 12 ± 1.1% at 1 mol L^{-1} NaCl. Sorption the NaOH system was much greater and was unaffected by solution ionic strength. Here again the pH of the system greatly increased as the concentration of NaOH increased. At 10^{-3} mol L^{-1} NaOH (pH 6.1), 80% of the Sr was sorbed to the sediment. This increased to 89 ± 0.2% at 10^{-2} mol L^{-1} NaOH (pH 11.6) but decreased to 60% at 10^{-1} mol L^{-1} NaOH. The total Sr sorption however then increased back to 80% at 1 mol L^{-1} NaOH (pH 13.8).

3.2EXAFS

EXAFS spectra were gathered for the illite system from samples exposed to a NaOH background at 10^{-5} mol L^{-1} (pH 8.9), 10^{-3} mol L^{-1} (pH 9.2), 10^{-1} mol L (pH 13), and 1 mol L^{-1} (pH 13.7). The resulting spectra and their Fourier transforms are shown in Figure 2, where the dotted line represents the best shell by shell fit. The fit parameters are then shown in Table 1. The spectrum collected from the sample equilibrated in 10^{-5} mol L^{-1} NaOH (pH 8.9) was best fit by a single oxygen shell at 2.6 Å (Figure 2a). Again the spectrum from the 10^{-3} mol L^{-1} NaOH background (pH 9.2) sample was best fit with a single O shell at 2.6 Å (Figure 2b). The 10^{-1} mol L NaOH background (pH 13) sample was also best fit with a single O shell, again at 2.6 Å (Figure 2c). In this case, an attempt was made to fit a Si/Al shell at 3.4 Å. This yielded a minor improvement in the fit, suggesting that a small portion of the Sr may be in a closer sorption environment. Note that it is not possible to differentiate between Si and Al backscatters in EXAFS. As both are present in the structure at this distance the shell is referred to as having either atom present (though Si was included in excurv in all cases). Finally shell by shell fitting was performed for the 1 mol L^{-1} NaOH background system (pH 13.7). Here the Sr–O interatomic distances and coordination numbers were refined to 2.7 Å, and 12, respectively, then fixed to these values. The fit was then greatly improved by the addition of a Si/Al shell of 12 atoms at 3.4 Å. Finally, the peak at 5 Å was initially fit with Sr as the coordinating atom. However, this failed to resolve satisfactorily and the fit statistics suggested a poor fit. Therefore, the possibility of a Sr precipitate at the edge of the illite was rejected. Due to this lack of precipitate formation the Sr was most likely sorbing into the illite interlayer, where the dominant interlayer cation would be K. Therefore, a shell of 6 K atoms at 5 Å was added and the number and identity of atoms in each shell was then fixed (based on the crystallographic structure of the interlayer). The shell filling was then improved be refinement of the Debye–Waller factor alone. In this case a best fit was given by an O shell at 2.7 Å, a Si/Al shell at 3.4 Å and a K shell at 5.0 Å (Table 1 and Figure 2 d).

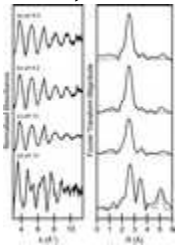

Figure 2. Sr k-space EXAFS and accompanying Fourier transform of Sr sorbed to ilite at (a) pH 8.9, (b) pH 9.2, (c) pH 13, and (d) pH 14. Solid lines are background subtracted data, and dashed lines are refined model fits.

Table 1. EXAFS Fitting Parameters for Sr Sorbed to Illite under Different pH Conditions[a]

sample	shell	n	r (Å)	$2\sigma^2$ (Å^2)	R
illite pH 8.9*	O	9	2.61	0.021	25.6
illite pH 8.9	O	8.6	2.611	0.02	24.95
	Si/Al	0.7	3.391	0.031	
illite pH 9.2*	O	9.2	2.609	0.022	19.25
illite pH 9.2	O	8.9	2.61	0.022	18.9
	Si/Al	0.6	3.34	0.041	
illite pH 13	O	9	2.604	0.03	24.63
illite pH 13*	O	8.4	2.607	0.027	22.39
	Si/Al	1	3.331	0.024	
illite pH 14	O	12	2.697	0.024	58.61
illite pH 14	O	12	2.716	0.023	49.25
	Si/Al	12	3.388	0.035	
illite pH 14	O	12	2.722	0.023	49.58
	Si/Al	12	3.395	0.034	
	Sr	6	5.344	0.060	
illite pH 14*	O	12	2.725	0.023	38.61
	Si/Al	12	3.396	0.033	
	K	6	5.038	0.014	

a

n, shell occupancy (±25%); r, interatomic distance (±0.02 Å for first shell and ±0.05 Å for subsequent shells); $2\sigma^2$, Debye–Waller factor (±25%); R, least squared residual. Final accepted (and plotted) fits are marked with an asterisk (*).

Sr K-edge EXAFS spectra were gathered from the chlorite system at four different concentrations of NaOH. Specifically, these were 10^{-5} mol L^{-1} (pH 9.0), 10^{-3} mol L^{-1} (pH 10.7), 10^{-1} mol L^{-1} (pH 12.9), and 1 mol L^{-1} (pH 13.8) NaOH background. Figure 3 shows the background subtracted EXAFS and their accompanying Fourier transforms. Here the solid lines represent the recorded data and the dotted lines are the best fits discovered from shell by shell fitting. The accompanying fit parameters for the chlorite system are shown in Table 2. The EXAFS spectrum for Sr sorbed to chlorite from the 10^{-5} mol L^{-1} NaOH system (pH 9.0) was best fitted with a single oxygen shell at 2.6 Å (Figure 3a). Again, in the 10^{-3} mol L^{-1} NaOH background, the Sr EXAFS spectrum was best fitted with a single oxygen shell at 2.6 Å (Figure 3b). For the 10^{-1} mol L^{-1} NaOH background system (pH 12.9), a single oxygen shell failed to provide the best fit to the recorded spectrum (see Table 2). The fit was significantly improved by adding an additional Si/Al shell at 3.8 Å, and this is shown in Figure 3d. Finally, in the 1 mol L^{-1} (pH 13.8) NaOH background, the spectrum was fit with the same two-shell model as the pH 12.9 sample. In this case, the addition of a Si/Al shell at 3.8 Å gave minimal improvement in the overall quality of the fit (Table 2). However, there was a trend within the sample for increasing shell number with increasing pH. This correlates

with the formation of an inner sphere complex and selective sorption at high pH (see Figure 1b). Therefore, it is consistent with other results from the chlorite system for Sr to fit with two shells at this pH.

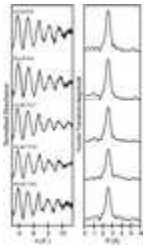

Figure 3. Sr k-space EXAFS and accompanying Fourier transform of Sr sorbed to chlorite at (a) pH 6.6, (b) pH 9.0, (c) pH 10.7, (d) pH 12.9, and (e) pH 13.8. Solid lines are background subtracted data, and dashed lines are refined model fits.

Table 2. EXAFS Fitting Parameters for Sr Sorbed to Chlorite under Different pH Conditions[a]

sample	shell	n	r (Å)	$2\sigma^2$ (Å^2)	R
chlorite pH 6.6*	O	9.1	2.602	0.018	22.35
chlorite pH 9*	O	9	2.591	0.019	27.41
chlorite pH 10.7*	O	9.2	2.607	0.022	15.56
chlorite pH 12.9	O	8.7	2.599	0.025	20.74
chlorite pH 12.9*	O	8.4	2.604	0.024	15.3
	Si/Al	1.2	3.783	0.012	
chlorite pH 13.8	O	8.8	2.626	0.021	30.86
chlorite pH 13.8*	O	9.1	2.624	0.022	30.03
	Si/Al	2	3.805	0.021	

a

n, shell occupancy (±25%); r, interatomic distance (±0.02 Å for first shell and ±0.05 Å for subsequent shells); $2\sigma^2$, Debye–Waller factor (±25%); R, least squared residual. Final accepted (and plotted) fits are marked with an asterisk (*).

For goethite, as with the previous minerals, representative samples were selected from the NaOH system and Sr EXAFS spectra collected to determine the bonding environment. Figure 4 shows the Sr EXAFS spectra and the Fourier transforms with their associated fits for the goethite system. The fit parameters for the shell by shell fits are shown in Table 3. Figure 4a shows the spectra obtained for Sr sorption to goethite in a background of 10^{-5} mol L^{-1} (pH 7.7). Here the best modeled fit was obtained with a single O shell at 2.6 Å. The spectrum for Sr sorption to goethite in 10^{-1} mol L^{-1} NaOH is shown in Figure 4b. In this case, an O shell at 2.6 Å and a Fe shell at 3.6 Å provided the simplest best fit to the spectra (Figure 4b). Evidence from the Fourier transform supports a second Fe shell at 4.5 Å; however, the addition of this backscatterer did not significantly improve the overall fit validity (Table 3). Finally, for the 10^{-1} NaOH background (pH 13.7 the best fit was given by an O shell at 2.6 Å and single Fe shell at 3.6 Å (Figure 4c). There was no evidence of a second Fe shell.

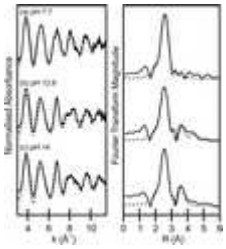

Figure 4. Sr k-space EXAFS and accompanying Fourier transform of Sr sorbed to goethite at (a) pH 7.7, (b) pH 12.6, and (c) pH 14.0. Solid lines are background subtracted data, and dashed lines are refined model fits.

Table 3. EXAFS Fitting Parameters for Sr Sorbed to Goethite under Different pH Conditions[a]

sample	shell	n	r (Å)	$2\sigma^2$ (Å^2)	R
goethite pH 7.7*	O	9	2.602	0.019	32.57
goethite pH 12.6	O	8.9	2.596	0.027	48.74
goethite pH 12.6	O	9	2.601	0.024	42.91
	Fe	3.2	3.596	0.028	
goethite pH 12.6*	O	8.1	2.599	0.021	38.68
	Fe	2.9	3.598	0.027	
	Fe	3.3	4.479	0.029	
goethite pH 13.8*	O	8.6	2.602	0.021	38.32
	Fe	3.5	3.563	0.027	

a

n, shell occupancy (±25%); r, interatomic distance (±0.02 Å for first shell and ±0.05 Å for subsequent shells); $2\sigma^2$, Debye–Waller factor (±25%); R, least squared residual. Final accepted (and plotted) fits are marked with an asterisk (*).

Finally, Sr K-edge EXAFS were gathered for the 10^{-1} mol L^{-1} (pH 13) and 1 mol L^{-1} (pH 13.8) sediment samples. The EXAFS spectra and associated Fourier transforms are shown in Figure 5. In both cases, a single and double shell fit were tried. For the 10^{-1} mol L^{-1} sample, a single oxygen shell was fitted at 2.6 Å with a resulting Debye–Waller factor of 0.031. In this sample, the addition of a Si/Al shell at 3.8 Å significantly improved the overall fit quality; it is this final two-shell fit which is displayed in Figure 5a. The fit parameters for both the one-shell and two-shell fit are shown in Table 4. Again, in the case of the 1 mol L^{-1} sediment sample (Figure 5b), the best fit was obtained with two shells. An oxygen shell was fitted at 2.6 Å and a Si/Al shell, again at 3.8 Å. Again, in this case, the addition of a Si/Al shell significantly improved the overall fit (Table 4).

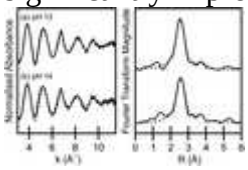

Figure 5. Sr k-space EXAFS and accompanying Fourier transform of Sr sorbed to a mixed phase sediment at (a) pH 13.0 and (b) pH 14.0. Solid lines are background subtracted data, and dashed lines are refined model fits.

Table 4. EXAFS Fitting PArameters for Sr Sorbed to the Mixed Phase Sediment under Different pH Conditions[a]

sample	shell	n	r (Å)	$2\sigma^2$ (Å^2)	R
sediment pH 13	O	9.1	2.603	0.031	21.84
sediment pH 13*	O	8	2.599	0.026	16.42
	Si/Al	1.4	3.81	0.016	
sediment pH 14	O	8.1	2.616	0.029	34.18
sediment pH 14*	O	7.5	2.613	0.026	32.96
	Si/Al	1.4	3.816	0.017	

a

n, shell occupancy (±25%); r, interatomic distance (±0.02 Å for first shell and ±0.05 Å for subsequent shells); $2\sigma^2$, Debye–Waller factor (± 25%); R, least squared residual. Final accepted (and plotted) fits are marked with an asterisk (*).

-

4 Discussion

4.1Effect of pH on Sr Sorption

The solution sorption data (Figure 1) indicates that in a NaCl solution at a slightly alkaline pH Sr sorbs through formation of outer-sphere surface complexes on all minerals. In this system, both the Na^+ and Sr^{2+} ions are competing for the same charged surface sites on all the minerals. The sorption is nonselective and controlled only by equilibrium reactions of both ions between the surface and solution. These can be expressed as the following half reactions for both the clay minerals:$2S^- + Sr^{2+} = 2S^-\cdots Sr^{2+}(1)S^- + Sr^{2+} = S^-\cdots Sr^{2+}(2)S^- + Na^+ = S^-\cdots Na^+$(3)Here, S is the permanently charged surface site and $\cdots$ denotes an electrostatic bond. Specifically, for the clays (illite and chlorite), these are negatively charged areas of the basal plane surface which have a net negative charge due to isomorphic substitutions within the aluminosilicate lattice.

Unlike the clay minerals goethite does not possess any permanent charge sites. Instead its surface charge is pH dependent, and protonates or deprotonates according the solution pH, yielding negatively charged OH groups above the point of zero charge (PZC; pH 7.5).(38) The cations are then attracted to form outer-sphere complexes.$2S(OH) + Sr^{2+} = 2S(OH)\cdots Sr^{2+}$(4) $S(OH) + Na^+ = S(OH)\cdots Na^+$(5)Each site carries a single charge; therefore, when Sr^{2+} sorbs, either the net negative charge on the hydrated ion is balanced by two charged sites on the surface (eqs 1 and 4) or it remains with one net positive charge which is distributed among its waters of hydration (eq 2). Na^+ is charged balanced by a single negatively charged site (eqs 3 and 5). As all these interactions are outer-sphere, the ions remain hydrated and the concentrations of each ion on the surface is governed solely by the law of mass action in competition with each other as below:$S^-\cdots Na + Sr^{2+} \leftrightarrow S^-\cdots Sr^+ + Na^+(6)2S(OH)\cdots Na + Sr^{2+} \leftrightarrow 2S(OH)\cdots Sr^{2+} + 2Na^+$(7) When the ionic strength of Na in solution increases, the equilibrium reaction is shifted to increase Na sorption to the mineral surface. Therefore, Na out-competes Sr and the total Sr surface concentration decreases (resulting in a decrease in % sorption). However, in the NaOH system, the increasing concentration of Na is accompanied by an increase in the solution pH. Here, as the Na concentration increases, it does not compete with Sr and the Sr sorption remains as high as in the low ionic strength experiments, indicating the formation of

a specifically sorbed inner-sphere surface complex. This phenomenon was observed in all the mineral systems, indicating that it is likely to be caused by the chemistry of the solution, rather than any nature of the sorption site. Although previous authors have showed the formation of the Sr-zeolite type phase under these high pH conditions the bond distances and occupancies they proposed are quite different from those found in the current study(39-41) (see the Supporting Information). This further supports that the Sr is still sorbing to the surface rather than forming any new precipitate. This is likely due to the short time period of the experiments (see Introduction).

4.2EXAFS Analysis of Sr Sorption at High pH

The specific sorption of Sr onto the minerals at high pH suggests there was a change in the sorption mechanism and that Sr was no longer sorbing in an outer-sphere complex in competition with Na. To investigate this, EXAFS spectra were collected for Sr across the pH range and onto each of the three minerals (and the mixed sediment). The measured EXAFS spectra and Fourier transforms for the four mineral systems are shown in Figures 2–5, and the EXAFS fit parameters in Tables 1–4. The first thing that is apparent from the fits is that below pH 12.5–13 the Sr is sorbing to all the minerals with a single oxygen shell. This is identical to the solution species(9, 39) and indicative of the formation an outer-sphere surface complex, as was seen in the NaCl system (above). Strontium held in these outer-sphere complexes is in thermodynamic equilibrium with the solution and any competing ions in solution. This therefore explains why increasing ionic strength (in the NaCl system) at this moderate pH led to a reduction in strontium sorption. This process of outer-sphere sorption has been widely observed and discussed by other authors and is thought to account for Sr mobility in the environment.(3, 5, 7)

The novelty of this current study becomes apparent in those EXAFS spectra obtained from Sr sorbed at extremely high pH and ionic strength. Here the sorption mechanism for Sr changes from showing a single oxygen shell to multiple coordination shells. These multiple shells are indicative of the formation of an inner-sphere complex.(19, 25) This change in sorption mechanism was seen in all three of the mineral systems, however the nature of the surface site was noticeably different.

First, Sr showed two distinct inner-sphere sorption environments on illite at pH 13 (Figure 2c) and pH 14 (Figure 2d). Specifically, at pH 13, the best fit for the EXAFS was obtained with both an oxygen shell at 2.6 Å and Si (Al) shell at 3.3 Å. Although the improvement in fit by adding a second shell was quite small (∼9%) compared to the one shell model (Table 1). The percentage sorption in the pH 13 NaOH experiment is greater (∼80% versus ∼40%) than the NaCl experiment (pH 9) at the same ionic strength (Figure 1a), indicating ion-specific adsorption of Sr at this pH. Therefore, including the possibility of inner sphere sorption must be considered even though the EXAFS evidence for an inner sphere coordination environment is weak. This is consistent with the inner-sphere surface complex observed by Wallace et al.(24) for Sr adsorption to a mixed sediment from a KOH dominated high pH solution. Therefore, it is proposed that the high pH of this system has altered the sorption mechanism of Sr. Rather than sorbing via cation exchange, it has become specifically adsorbed to the surface. At pH 14, the EXAFS data shows that Sr is sorbed to illite via a different incorporation mechanism. The EXAFS spectrum collected from this sample (Figure 2d) was best fitted by three coordination shells, specifically a shell of 12 oxygens at 2.7 Å, a Si/Al shell at 3.4 Å and an additional K shell at 5.0 Å. Based on the crystallographic structure of illite the only place where strontium could be held in this coordination environment is within the illite interlayer. Here the Sr is surrounded by 6 O atoms from each tetrahedral layer on either side of the interlayer, giving a total of 12. The lengthening of the Sr–O distance from 2.6 Å, as seen in all other fits, to 2.7 Å, is indicative of the fact that the Sr was incorporated, rather than sorbed. The 12 Si/Al atoms at 3.4 Å result from the tetrahedral

layers (6 from each sheet). This high coordination number is not possible if the Sr was simply adsorbed on the surface or the edge. Finally, the coordinating atoms at 5 Å were shown to be best fit to K rather than Sr, indicating incorporation into the interlayer. Therefore, in this system, Sr is becoming incorporated into the interlayer structure of the illite mineral. This mechanism has been previously observed for monovalent alkali ions (such as K and Cs)(1, 21, 42-44) but was not previously known to occur for divalent alkaline-earths. It has previously been thought that the large hydration energy of the alkaline earths (such as Sr^{2+} and Ca^{2+}) meant they would only enter into the interlayer while remaining hydrated in outer-sphere complexes (as was seen at pH 9; Figure 2a).(45-47) However, this new result indicates that at high pH Sr can shed its hydration shell and become incorporated into the illite interlayer.

The EXAFS spectra indicated that Sr sorption to chlorite showed a very similar trend to illite. This is understandable as they are both aluminosilicate clay minerals. Again, at pH 12.9 (Figure 3d), the inclusion of a Si/Al shell at 3.7 Å significantly improved the model fit. This coordination environment was best described by the same inner-sphere surface complex. This same two shell fit also proved the best fit for Sr sorbed to chlorite at pH 13.8 (Figure 3e). This difference from the illite system is due to the mineralogical variation between illite and chlorite. Chlorite does not have an ion filled interlayer, but instead has its 2:1 layers separated by a brucite-like layer.(48, 49) Therefore, the interlayer incorporation of Sr seen in illite at pH 14 was not possible as these sorption sites are not present on chlorite. Therefore, the Sr was likely sorbing via inner-sphere surface complexation onto the basal surface, or at the edge of the interlayer. This ion-specific incorporation again explains why the Sr sorption percentage was so high, even in a high ionic strength background solution.

The goethite system showed a change in the sorption coordination environment at both pH 12.6 and 14 (Figure 4c and d). At pH 12.6, the Sr is coordinated by a double Fe shell (at 2.9 and 3.3 Å), indicative of an inner-sphere complex. This is not present at pH 7.7 where Sr is present in an outer-sphere complex. At pH 14, the Sr again appears to be coordinated in an inner-sphere complex but with a single close Fe shell (at 3.6 Å). This suggests that the Sr is forming an alternative inner-sphere complex at a different reactive site on the goethite surface to that formed at pH 12.6. This inner-sphere surface complexation on goethite was previously observed by Collins et al.(25) at pH 10.2 but fitted by a single Fe shell at 4.3 Å. Therefore, it appears that the Sr atom migrates into a closer complex as the pH of the background solution increases.

Finally, the coordination environment of Sr onto sediment at hyper-alkaline pH was tested as a real world analogue. The sediment investigated was the same as that used by Wallace et al.(24) and is analogous to that underlying the UK Sellafield site. Although the sediment is known to contain all the minerals investigated here,(29, 30, 50) chlorite dominates the reactive surface area.(24) The EXAFS spectra for the pH 13 and 14 samples (Figure 5) show that in both cases Sr was held in an inner-sphere surface complex coordinated by an O shell at 2.6 Å and a Si/Al shell at 3.8 Å. This most closely matches the bonding environment found for Sr on the surface of chlorite and therefore suggests that chlorite is the dominant phase controlling Sr sorption in these sediments (at hyper alkaline pH).

4.3Sorption mechanism

All the experiments conducted here were performed at a pH range above the point of zero charge for all the minerals; specifically, the pH PZC is 2.5 for illite, 3 for chlorite,(51) and around 7.5 for goethite.(38) However, as the pH of the system increases, the amphoteric sites on the surface will become increasingly deprotonated, making the surface more negative and allowing the possibility of direct bonding to the deprotonated surface oxygens.

It has already been shown from the illite EXAFS that at hyperalkaline pH Sr appears to behave as a monovalent rather than a divalent cation. Strontium is known to exist in the

aqueous phase as two species. The divalent Sr^{2+} ion is dominant under most pH conditions. However, at hyperalkaline pH, Sr is known to form the monovalent $SrOH^+$ species in solution.(52) This presence of $SrOH^+$ as the dominant species in solution could offer a mechanistic explanation for the formation of inner-sphere surface complexes in these hyperalkaline systems. Specifically, it is likely that the following complexes are forming on each mineral phase$$S^- + (SrOH)^+ = S{-}SrOH \quad (8)$$where S is the basal surface of the both illite and chlorite. This is the likely dominant complex at pH 12–13 on these minerals and $$EO^- + (SrOH)^+ = EO{-}SrOH \quad (9)$$where E are the hanging hydroxyl groups at the edge of the chlorite lattice. This is the likely inner-sphere sorption site seen in the chlorite system. This same sorption site may also be occurring in the pH 13 illite system. However, it is impossible to differentiate the exact location of the inner-sphere complex.

In the goethite, the $SrOH^+$ is likely sorbing onto the surface hydroxyls, yielding $$SO^- + (SrOH)^+ = SO{-}SrOH \quad (10)$$These inner-sphere complexes on the amphoteric edge and goethite surface sites can only form when those sites are fully deprotonated at very high pH, explaining their existence in the highest pH treatment only.

Finally, in the case of the illite interlayer, the following structure likely exists $$SO{-}K{-}OS + (SrOH)^+ = SO{-}SrOH{-}OS + K^+ \quad (11)$$Here the monovalent $SrOH^+$ is able to exchange with the movovalent K^+ ion in the interlayer, yielding a S–O–Sr bond where S is the Si/Al tetrahedra.

If the other alkali-earth ions show the same solution speciation behavior, it is possible that they would also sorb via the same mechanism as Sr. To test this hypothesis, PHREEQC was used to model the speciation of four important alkaline earth ions, namely, Ca, Sr, Ba, and Ra. Sr was chosen as it is investigated in this study. The decision was taken to also investigate Ca, Ba, and Ra, as these are important elements that are relevant to the disposal of nuclear wastes (Ca is the dominant ion in many types of cement leachate; Ra is an important long-lived radionuclide; and Ba is often used as an analogue for Ra).(16, 53) The modeling results (Figure 6) showed that Ca, Sr, and Ba all formed a hydroxide species within the pH range investigated, but that Ra was only present as Ra^{2+}. However, the pH at which the hydroxyl species became dominant varied between the different elements. Strontium began to speciate as $SrOH^+$ above pH 11.5 and became the dominant solution species above pH 13.7 (Figure 6b). The EXAFS investigations showed that the inner-sphere complexes did not form at pHs below 11 (e.g., Figure 2c) but were readily apparent above 12.5. This strongly suggests that the speciation of Sr from a 2+ to a 1+ cation allows it to form inner-sphere surface complexes. All of the tested minerals have hydroxyl groups present on their surfaces. Therefore, at elevated pH, the Sr is potentially sorbing into inner sphere complexes via ligand exchange of its aqueous OH^- group for the OH^- present on the surface of the minerals. Interestingly, the $SrOH^+$ is only incorporated into illite when it is the dominant solution species. It has been widely reported that Cs^+ and other monovalent alkali cations are selectively incorporated into inner-sphere complexes in the illite interlayer.(43, 54, 55) Cs is known to be selectively retained in this interlayer site.(44) Therefore, it would be valuable to investigate whether, once incorporated, Sr was also retained in the illite interlayer across a range of pH and IS conditions.

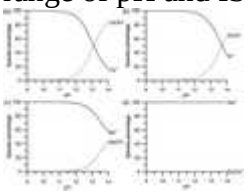

Figure 6. Speciation of four alkali earth elements as a function of pH determined by PHREEQC modeling: (a) Ca^{2+} and $CaOH^{+}$; (b) Sr^{2+} and $SrOH^{+}$; (c) Ba^{2+} and $BaOH^{+}$; and (d) Ra^{2+} and $RaOH^{+}$.

4.4Implications for Radionuclide Behavior

The conclusion that it is the speciation of Sr into the $SrOH^{+}$ species that is responsible for its inner-sphere incorporation and retention has important implications for the behavior of the other ions modeled. Both Ca and Ra are expected to be present in solutions at cementitious geological disposal facilities for radioactive waste. Radium, as a long-lived radionuclide, is present in the waste and Ca is abundant when leached from the cementitious backfill. The interaction of this backfill with groundwater is expected to yield high pH high ionic strength solution, known as young cement water.(16, 24) Therefore, it is essential to understand the sorption behavior of these important elements in high pH and IS environments. Due to the high radiotoxicity of Ra, Ba is often used as a inactive analogue in experiments.(56) The modeling results (Figure 6) show two important points. First, in this high pH and high IS environment, the $CaOH^{+}$ species will dominate. EXAFS data reported here has shown that (for $SrOH^{+}$) these monovalent hydroxyl species can sorb in inner-sphere complexes. If $CaOH^{+}$ can form inner-sphere complexes in the same way as $SrOH^{+}$, significant concentrations of Ca may be sorbed onto mineral surfaces at high pH. This would reduce the total concentration of Ca in solution. Current predictions of radionuclide migration assume a given concentration of Ca.(57, 58) These results show that sorption of $CaOH^{+}$ may reduce the total solution concentration and may have implications for precipitation of U and Ra bearing carbonate phases.(56, 57) Second the modeling shows that while Ba forms a $BaOH^{+}$ species, which may also sorb via inner-sphere complexation; Ra remains as Ra^{2+} which would only be bound via cation exchange. Therefore, the sorption of Ba in high IS, high pH systems may be greater than for Ra. Analogue experiments using Ba may therefore underestimate the concentration of Ra remaining mobile in the aqueous phase.

-

5 Conclusions

Here it has been shown from batch sorption experiments and EXAFS spectroscopy that under conditions of high ionic strength and high pH, Sr is selectively retained on charged surfaces of minerals. Under low pH conditions, Sr speciates as the divalent Sr^{2+} cation which sorbs in outer-sphere complexes. This occurs in competition with other monovalent and divalent cations and is strongly controlled by solution ionic strength with Sr sorption reducing with increasing ionic strength. At high pH, however, the monovalent $SrOH^{+}$ ion dominates in solution. This Sr species adsorbs via inner-sphere surface complexation and allows the retention of Sr on charged surface sites even when high concentrations of competing ions are present.

Supporting Information

The Supporting Information is available free of charge on the ACS Publications website at DOI: 10.1021/acs.langmuir.5b04633.

- XRD spectra of starting materials; Sr sorption to sediment at pH 6.5; comparative EXAFS spectra (PDF)

‖Author Present Address

AJ.F.: Centre for Radiochemistry Research, School of Chemistry, University of Manchester, Manchester M13 9PL, United Kingdom.

The authors declare no competing financial interest.

-

Acknowledgment

The authors wish to thank Paul Lythgoe for support with ICP analysis. This work was primarily funded by the UK Engineering and Physical Sciences Research Council (EPSRC) industrial CASE Studentship #10000173 in partnership with National Nuclear Laboratory awarded to A.J.F. Sr K-edge EXAFS were gathered at three separate beamline sessions at beamlines B18 (proposal SP8667) and I20 (proposal SP2471) at the Diamond Light Source, Didcot, UK and at the Dutch Belgian Beamline (BM26A) (proposal EV-15) at the European Synchrotron Radiation Facility, Grenoble, France.

- Reference QuickView
-

References

This article references 58 other publications.

1. **1.**

   Dyer, A.; Chow, J. K. K.; Umar, I. M.The uptake of caesium and strontium radioisotopes onto clays J. Mater. Chem. 2000, 10 (12) 2734– 2740, DOI: 10.1039/b006662l

   [CrossRef], [CAS]

2. **2.**

   Balek, V.; Málek, Z.; Šubrt, J.; Ždimera, A.Characterization of iron(III) oxide and oxide-hydroxide as Sr-sorbent J. Radioanal. Nucl. Chem. 1996, 212 (5) 321– 331, DOI: 10.1007/BF02162647

   [CrossRef], [CAS]

3. **3.**

Carroll, S. A.; Roberts, S. K.; Criscenti, L. J.; O'Day, P. A.Surface complexation model for strontium sorption to amorphous silica and goethite Geochem. Trans. 2008, 9, 2, DOI: 10.1186/1467-4866-9-2

[CrossRef], [PubMed], [CAS]

4. **4.**

Karasyova, O. N.; Ivanova, L. I.; Lakshtanov, L. Z.; Lövgren, L.Strontium Sorption on Hematite at Elevated Temperatures J. Colloid Interface Sci. 1999, 220 (2) 419– 428, DOI: 10.1006/jcis.1999.6474

[CrossRef], [PubMed], [CAS]

5. **5.**

Axe, L.; Bunker, G. B.; Anderson, P. R.; Tyson, T. A.An XAFS analysis of strontium at the hydrous ferric oxide surface J. Colloid Interface Sci. 1998, 199 (1) 44– 52, DOI: 10.1006/jcis.1997.5347

[CrossRef], [CAS]

6. **6.**

Chen, C. C.; Hayes, K. F.X-ray absorption spectroscopy investigation of aqueous Co(II) and Sr(II) sorption at clay-water interfaces Geochim. Cosmochim. Acta 1999, 63 (19–20) 3205– 3215, DOI: 10.1016/S0016-7037(99)00245-8

[CrossRef], [CAS]

7. **7.**

Parkman, R. H.; Charnock, J. M.; Livens, F. R.; Vaughan, D. J.A study of the interaction of strontium ions in aqueous solution with the surfaces of calcite and kaolinite Geochim. Cosmochim. Acta 1998, 62 (9) 1481– 1492, DOI: 10.1016/S0016-7037(98)00072-6

[CrossRef], [CAS]

8. **8.**

Chen, C. C.; Coleman, M. L.; Katz, L. E.Bridging the gap between macroscopic and spectroscopic studies of metal ion sorption at the oxide/water interface: Sr(II), Co(II), and Pb(II) sorption to quartz Environ. Sci. Technol. 2006, 40 (1) 142– 148, DOI: 10.1021/es050356g

[ACS Full Text], [PubMed], [CAS]

9. **9.**

Sahai, N.; Carroll, S. A.; Roberts, S.; O'Day, P. A.X-ray absorption spectroscopy of strontium(II) coordination - II. Sorption and precipitation at kaolinite, amorphous silica, and goethite surfaces J. Colloid Interface Sci. 2000, 222 (2) 198– 212, DOI: 10.1006/jcis.1999.6562

[CrossRef], [PubMed], [CAS]

10. **10.**

Torstenfelt, B.; Andersson, K.; Allard, B.Sorption of Strontium and Cesium on Rocks and Minerals Chem. Geol. 1982, 36, 123– 137, DOI: 10.1016/0009-2541(82)90042-0

[CrossRef], [CAS]

11. **11.**

Bilgin, B.; Atun, G.; Keceli, G.Adsorption of strontium on illite J. Radioanal. Nucl. Chem. 2001, 250 (2) 323– 328, DOI: 10.1023/A:1017960015760

[CrossRef], [CAS]

12. **12.**

Khan, S. A.; RiazurRehman; Khan, M. A.Sorption of strontium on bentonite Waste Manage. (Oxford, U. K.) 1995, 15 (8) 641– 650, DOI: 10.1016/0956-053X(96)00049-9

[CrossRef]

13. **13.**

SellafieldLtd. Generic Basics for Inventory Challenge - Legacy Alkaline Sludge Systems; Sellafield Ltd: Cumbria, UK, 2009.

14. **14.**

Ahearne, J. F.Radioactive waste: The size of the problem Phys. Today 1997, 50 (6) 24– 29, DOI: 10.1063/1.881763

[CrossRef], [CAS]

15. **15.**

Savage, D.A review of analogues of alkaline alteration with regard to long-term barrier performance Mineral. Mag. 2011, 75 (4) 2401– 2418, DOI: 10.1180/minmag.2011.075.4.2401

[CrossRef], [CAS]

16. **16.**

Fernández, R.; Mäder, U. K.; Rodríguez, M.; De La Villa, R. V.; Cuevas, J.Alteration of compacted bentonite by diffusion of highly alkaline solutions Eur. J. Mineral. 2009, 21 (4) 725– 735, DOI: 10.1127/0935-1221/2009/0021-1947

[CrossRef], [CAS]

17. **17.**

Tits, J.; Wieland, E.; Dobler, J. P.; Kunz, D.; Oversby, V. M.; Werme, L. O.The uptake of strontium by calcium silicate hydrates under high pH conditions: An experimental approach to distinguish adsorption from Co-precipitation processes MRS Proc. 2004, 689– 694, DOI: 10.1557/PROC-807-A101

[CrossRef], [CAS]

18. **18.**

Zhao, H.; Deng, Y.; Harsh, J. B.; Flury, M.; Boyle, J. S.Alteration of kaolinite to Cancrinite and sodalite by simulated Hanford tank waste and its impact on cesium retention Clays Clay Miner. 2004, 52 (1) 1– 13, DOI: 10.1346/CCMN.2004.0520101

[CrossRef], [CAS]

19. **19.**

Tits, J.; Wieland, E.; Müller, C. J.; Landesman, C.; Bradbury, M. H.Strontium binding by calcium silicate hydrates J. Colloid Interface Sci. 2006, 300 (1) 78– 87, DOI: 10.1016/j.jcis.2006.03.043

[CrossRef], [PubMed], [CAS]

20. **20.**

Wieland, E.; Tits, J.; Kunz, D.; Dähn, R.Strontium uptake by cementitious materials Environ. Sci. Technol. 2008, 42 (2) 403– 409, DOI: 10.1021/es071227y

[ACS Full Text], [PubMed], [CAS]

21. **21.**

Chorover, J.; Choi, S.; Rotenberg, P.; Serne, R. J.; Rivera, N.; Strepka, C.; Thompson, A.; Mueller, K. T.; O'Day, P. A.Silicon control of strontium and cesium partitioning in hydroxide-weathered sediments Geochim. Cosmochim. Acta 2008, 72 (8) 2024– 2047, DOI: 10.1016/j.gca.2008.01.026

[CrossRef], [CAS]

22. **22.**

Choi, S.; O'Day, P. A.; Rivera, N. A.; Mueller, K. T.; Vairavamurthy, M. A.; Seraphin, S.; Chorover, J.Strontium speciation during reaction of kaolinite with simulated tank-waste leachate: Bulk and microfocused EXAFS analysis Environ. Sci. Technol. 2006, 40 (8) 2608– 2614, DOI: 10.1021/es051869q

[ACS Full Text], [PubMed], [CAS]

23. **23.**

Chorover, J.; Choi, S.; Amistadi, M. K.; Karthikeyan, K. G.; Crosson, G.; Mueller, K. T.Linking cesium and strontium uptake to kaolinite weathering in simulated tank waste leachate Environ. Sci. Technol. 2003, 37 (10) 2200– 2208, DOI: 10.1021/es025980x

[ACS Full Text], [PubMed], [CAS]

24. **24.**

Wallace, S. H.; Shaw, S.; Morris, K.; Small, J. S.; Burke, I. T.Alteration of sediments by hyperalkaline k-rich cement leachate: Implications for strontium adsorption and incorporation Environ. Sci. Technol. 2013, 47 (8) 3694– 3700, DOI: 10.1021/es3051982

[ACS Full Text], [PubMed], [CAS]

25. **25.**

Collins, C. R.; Sherman, D. M.; Ragnarsdottir, K. V.The adsorption mechanism of Sr2+ on the surface of goethite Radiochim. Acta 1998, 81 (4) 201– 206, DOI: 10.1524/ract.1998.81.4.201

[CrossRef], [CAS]

26. **26.**

Hower, J.; Mowatt, T. C.The mineralogy of illites and mixed-layerillite/montmorillonites Am. Mineral. 1966, 51, 825– 854

[CAS]

27. **27.**

Martin, R. T.Reference chlorite characterization for chlorite identification in soil clays Clays Clay Miner. 1954, 3, 117, DOI: 10.1346/CCMN.1954.0030113

[CrossRef]

28. **28.**

Schwertmann, U.; Cornell, R. M. Iron Oxides in the Laboratory: Preparation and Characterisation; Wiley-VCH: Weinheim, 2000.

[CrossRef]

29. **29.**

Wallace, S. H.; Shaw, S.; Morris, K.; Small, J. S.; Fuller, A. J.; Burke, I. T.Effect of groundwater pH and ionic strength on strontium sorption in aquifer sediments: Implications for 90Sr mobility at contaminated nuclear sites Appl. Geochem. 2012, 27 (8) 1482– 1491, DOI: 10.1016/j.apgeochem.2012.04.007

[CrossRef], [CAS]

30. **30.**

Law, G. T. W.; Geissler, A.; Boothman, C.; Burke, I. T.; Livens, F. R.; Lloyd, J. R.; Morris, K.Role of Nitrate in Conditioning Aquifer Sediments for Technetium Bioreduction Environ. Sci. Technol. 2010, 44 (1) 150– 155, DOI: 10.1021/es9010866

[ACS Full Text], [PubMed], [CAS]

31. **31.**

Ravel, B.; Newville, M.ATHENA, ARTEMIS, HEPHAESTUS: data analysis for X-ray absorption spectroscopy using IFEFFIT J. Synchrotron Radiat. 2005, 12 (4) 537– 541, DOI: 10.1107/S0909049505012719

[CrossRef], [PubMed], [CAS]

32. **32.**

Tenderholt, A.; Hedman, B.; Hodgson, K. O.Pyspline: A modern, cross-platform program for the processing of raw averaged XAS edge and EXAFS data AIP Conf. Proc. 2006, 882, 105– 107, DOI: 10.1063/1.2644442

[CrossRef]

33. **33.**

Tomic, S.; Searle, B. G.; Wander, A.; Harrison, N. M.; Dent, A.; Mosselmans, J. F. W.; Inglesfield, J. E. New Tools for the Analysis of EXAFS: The DL_EXCURV Package; CCLRC: Daresbury, UK, 2005.

34. **34.**

Gurman, S. J.; Binsted, N.; Ross, I.A rapid, exact curved-wave theory for EXAFS calculations J. Phys. C: Solid State Phys. 1984, 17 (1) 143– 151, DOI: 10.1088/0022-3719/17/1/019

[CrossRef], [CAS]

35. **35.**

Binsted, N. EXCURV98: CLRC Daresbury Laboratory computer program; CLRC Daresbury: Warrington, 1998.

36. **36.**

Parkhurst, D. L.; Appelo, C. A. J. User's guide to PHREEQC, version 2; US Geological Survey: Denver, CO, 1999; Vol. 99-4259.

37. **37.**

Bond, K. A.; Heath, T. G.; Tweed, C. J. HATCHES: A Reference Thermodynamic Database for Chemical Equilibrium Studies; NSS/R379; NDA: Cumbria, UK, 1997.

38. **38.**

Cristiano, E.; Hu, Y.-J.; Siegfried, M.; Kaplan, D.; Nitsche, H.A COMPARISON OF POINT OF ZERO CHARGE MEASUREMENT METHODOLOGY Clays Clay Miner. 2011, 59 (2) 107– 115, DOI: 10.1346/CCMN.2011.0590201

[CrossRef], [CAS]

39. **39.**

O'Day, P. A.; Newville, M.; Neuhoff, P. S.; Sahai, N.; Carroll, S. A.X-ray absorption spectroscopy of strontium(II) coordination. I. Static and thermal disorder in crystalline, hydrated, and precipitated solids and in aqueous solution J. Colloid Interface Sci. 2000, 222 (2) 184– 197, DOI: 10.1006/jcis.1999.6621

[CrossRef], [PubMed], [CAS]

40. **40.**

Tamura, T.; Yoshiasa, A.; Iishi, K.; Takeno, S.; Maeda, H.; Emura, S.; Koto, K.Local structure of (Ca, Sr)2 (Mg, Co, Zn) Si2O7 melilite solid-solution with modulated structure Phys. Chem. Miner. 1996, 23 (2) 81– 88, DOI: 10.1007/BF00202302

[CrossRef], [CAS]

41. **41.**

Perdrial, N.; Rivera, N.; Thompson, A.; O'Day, P. A.; Chorover, J.Trace contaminant concentration affects mineral transformation and pollutant fate in hydroxide-weathered Hanford sediments J. Hazard. Mater. 2011, 197, 119– 127, DOI: 10.1016/j.jhazmat.2011.09.063

[CrossRef], [PubMed], [CAS]

42. **42.**

Poinssot, C.; Baeyens, B.; Bradbury, M. H.Experimental and modelling studies of caesium sorption on illite Geochim. Cosmochim. Acta 1999, 63 (19–20) 3217– 3227, DOI: 10.1016/S0016-7037(99)00246-X

[CrossRef], [CAS]

43. **43.**

Bostick, B. C.; Vairavamurthy, M. A.; Karthikeyan, K. G.; Chorover, J.Cesium adsorption on clay minerals: An EXAFS spectroscopic investigation Environ. Sci. Technol. 2002, 36 (12) 2670– 2676, DOI: 10.1021/es0156892

[ACS Full Text], [PubMed], [CAS]

44. **44.**

Fuller, A. J.; Shaw, S.; Ward, M. B.; Haigh, S. J.; Mosselmans, J. F. W.; Peacock, C. L.; Stackhouse, S.; Dent, A. J.; Trivedi, D.; Burke, I. T.Caesium incorporation and retention in illite interlayers Appl. Clay Sci. 2015, 108, 128– 134, DOI: 10.1016/j.clay.2015.02.008

[CrossRef], [CAS]

45. **45.**

Jackson, B. L. J.; During, C.Studies of slowly available potassium in soils of New Zealand - I. Effects of leaching, temperature and potassium depletion on the equilibrium concentration of potassium in solution Plant Soil 1979, 51 (2) 197– 204, DOI: 10.1007/BF02232883

[CrossRef], [CAS]

46. **46.**

Jackson, M. L. Weathering of Primary and Seondary Minerals in Soils. In 9th International Congress of Soil Science; The International Society of Soil Science and Angus & Robertson Ltd: Adelaide, Australia, 1968; Vol. IV, pp 281– 292.

47. **47.**

Sparks, D. L.; Huang, P. M. Physical Chemisty of Soil Potassium. In Potassium in Agriculture; Munson, R. D., Ed.; American Society of Agronomy: Madison, WI, 1985; pp 201– 276.

48. **48.**

Weaver, C. E.; Pollard, L. D. The chemistry of clay minerals; Elsevier: Amsterdam, 1973; Vol. 15.

49. **49.**

Grim, R. E. Clay Mineralogy; McGraw-Hill: New York, 1968.

50. **50.**

Thorpe, C. L.; Lloyd, J. R.; Law, G. T. W.; Burke, I. T.; Shaw, S.; Bryan, N. D.; Morris, K.Strontium sorption and precipitation behaviour during bioreduction in nitrate impacted sediments Chem. Geol. 2012, 306–307, 114– 122, DOI: 10.1016/j.chemgeo.2012.03.001

[CrossRef], [CAS]

51. **51.**

Hussain, S. A.; Demirci, G.; Özbayoğlu, G.Zeta Potential Measurements on Three Clays from Turkey and Effects of Clays on Coal Flotation J. Colloid Interface Sci. 1996, 184 (2) 535– 41, DOI: 10.1006/jcis.1996.0649

[CrossRef], [PubMed], [CAS]

52. **52.**

Takeno, N. Atlas of Eh-pH diagrams: Intercomparison of thermodynamics databases; National Institute of Advanced Industrial Science and Technology: Tokyo, 2005.

53. **53.**

De Windt, L.; Pellegrini, D.; Van Der Lee, J.Coupled modeling of cement/claystone interactions and radionuclide migration J. Contam. Hydrol. 2004, 68 (3–4) 165– 182, DOI: 10.1016/S0169-7722(03)00148-7

[CrossRef], [PubMed], [CAS]

54. **54.**

Sawhney, B. L.Selective Sorption and Fixation of Cations by Clay-Minerals - Review Clays Clay Miner. 1972, 20 (2) 93– 100, DOI: 10.1346/CCMN.1972.0200208

[CrossRef], [CAS]

55. **55.**

Eberl, D. D.Alkali cation selectivity and fixation by clay minerals Clays Clay Miner. 1980, 28 (3) 161– 172, DOI: 10.1346/CCMN.1980.0280301

[CrossRef], [CAS]

56. **56.**

Jones, M. J.; Butchins, L. J.; Charnock, J. M.; Pattrick, R. A. D.; Small, J. S.; Vaughan, D. J.; Wincott, P. L.; Livens, F. R.Reactions of radium and barium with the surfaces of carbonate minerals Appl. Geochem. 2011, 26 (7) 1231– 1238, DOI: 10.1016/j.apgeochem.2011.04.012

[CrossRef], [CAS]

57. **57.**

NDA. Geological Disposal: Radionuclide Behaviour Status Report; Nuclear Decommissioning Authority: Cumbria, UK, 2010.

58. **58.**

NDA. The 2010 UK Radioactive Waste Inventory; Nuclear Decommissioning Authority: Cumbria, UK, 2010.